Article

Promoting Vibrations in Human Purine Nucleoside Phosphorylase. A Molecular Dynamics and Hybrid Quantum Mechanical/Molecular Mechanical Study

Sara Nez, Dimitri Antoniou, Vern L. Schramm, and Steven D. Schwartz

J. Am. Chem. Soc., **2004**, 126 (48), 15720-15729• DOI: 10.1021/ja0457563 • Publication Date (Web): 05 November 2004

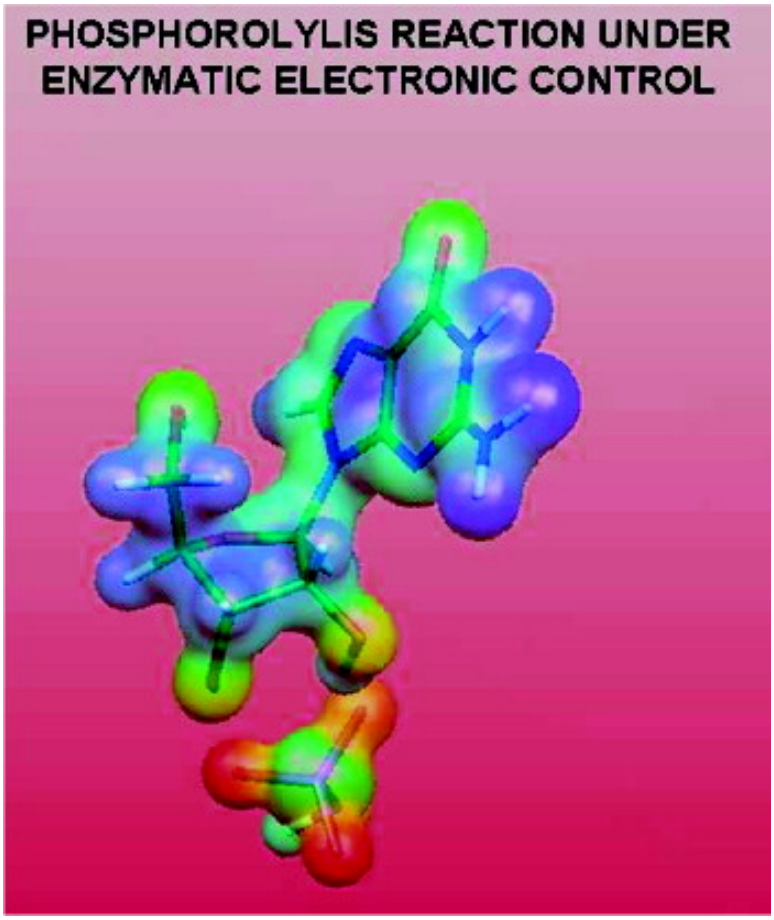

J|A|C|S
ARTICLES
Published on Web 11/05/2004

Promoting Vibrations in Human Purine Nucleoside Phosphorylase. A Molecular Dynamics and Hybrid Quantum Mechanical/Molecular Mechanical Study

Sara Núñez,[†,‡] Dimitri Antoniou,[‡] Vern L. Schramm,[†] and Steven D. Schwartz*[,†,‡]

Contribution from the Departments of Biochemistry and Biophysics, Albert Einstein College of Medicine, 1300 Morris Park Avenue, Bronx, New York 10461

Received July 15, 2004; E-mail: sschwartz@aecom.yu.edu

Abstract: Crystallographic studies of human purine nucleoside phosphorylase (hPNP) with several transition-state (TS) analogues in the immucillin family showed an unusual geometric arrangement of the atoms O-5′, O-4′, and O_P, the nucleophilic phosphate oxygen, lying in a close three-oxygen stack. These observations were corroborated by extensive experimental kinetic isotope effect analysis. We propose that protein-facilitated dynamic modes in hPNP cause this stack, centered on the ribosyl O-4′ oxygen, to squeeze together and push electrons toward the purine ring, stabilizing the oxacarbenium character of the TS. As the N-ribosidic bond is cleaved during the reaction, the pK_a values of N-7 and O-6 increase by the electron density expelled by the oxygen-stack compression toward the purine ring. Increased electron density in the purine ring improves electrostatic interactions with nearby residues and facilitates the abstraction of a proton from a solvent proton or an unidentified general acid, making the purine a better leaving group, and accelerating catalysis. Classical and mixed quantum/classical molecular dynamics (MD) simulations of the Michaelis complex of hPNP with the substrates guanosine and phosphate were performed to assess the existence of protein-promoting vibrations (PPVs). Analogous simulations were performed for the substrates in aqueous solution. In the catalytic site, the O-5′, O-4′, and O_P oxygens vibrate at frequencies of ca. 125 and 465 cm^{-1}, as opposed to 285 cm^{-1} in the absence of hPNP. The hybrid quantum mechanical/molecular mechanical method was used to assess whether this enzymatic vibration pushing the oxygens together is coupled to the reaction coordinate, and thus has a direct positive impact on catalysis. The potential energy surface for the phosphorolysis reaction for several snapshots taken from the classical MD simulation showed substantial differences in oxygen compression. Our calculations showed the existence of PPVs coupled to the reaction coordinate, which effect electronic alterations in the active site by pushing the three oxygen centers together in proximity, and accelerate substrate turnover in the phosphorolysis reaction catalyzed by hPNP.

Introduction

Human purine nucleoside phosphorylase (hPNP) is the only purine salvage enzyme that specifically catalyzes reversible bond cleavage of 6-oxopurine nucleosides to form phosphorylated α-D-ribose products in the presence of phosphate (Figure 1).[1]

In 1975, Giblett discovered that a child with a specific T-cell immunodeficiency was also deficient in hPNP.[2] All other tissues and cell types, including B-cells, were normal. The parents had normal immune function, but each had less than 50% of normal hPNP activity in erythrocytes. Analysis of metabolites from hPNP-deficient patients revealed a deficiency in uric acid formation together with increased circulating purine nucleosides and deoxynucleosides, and also overproduction of purines from the de novo pathways. It was later demonstrated that the biochemical link between hPNP and T-cell deficiency was the failure to degrade deoxyguanosine and its conversion to dGTP in activated T-cells.[3−6] Stimulated T-cells require DNA synthesis

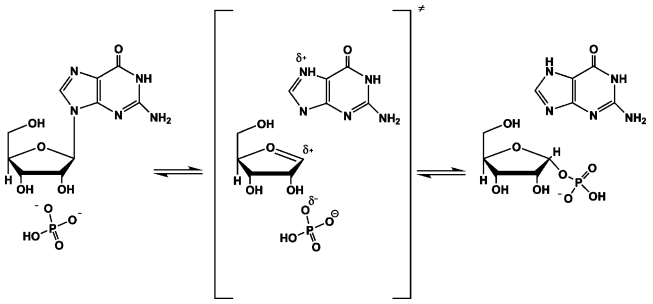

Figure 1. hPNP-catalyzed phosphorolysis of the purine nucleoside. The guanine leaving group and phosphate nucleophile are well-separated from the oxacarbenium ion, defining a highly dissociative TS.

[†] Department of Biochemistry.
[‡] Department of Biophysics.

(1) Stoeckler, J. D.; Cambor, C.; Parks, R. E. J. *Biochemistry* **1980**, *19*, 102−107.
(2) Giblett, E. R.; Ammann, A. J.; Wara, E. W.; Sandman, R.; Diamond, L. K. *Lancet I* **1975**, 1010−1013.
(3) Krenitsky, T. A.; Tuttlle, J. V.; Koszalka, G. W.; Chen, I. S.; Beachman, L. M.; Rideout, J. L.; Elion, G. B. *J. Biol. Chem.* **1976**, *251*, 4055−4061.
(4) Carson, D. A.; Kaye, J.; Seegmiller, J. E. *Proc. Natl. Acad. Sci. U.S.A.* **1977**, *74*, 5677−5681.
(5) Mitchell, B. S.; Mejias, E.; Daddona, P. E.; Kelly, W. N. *Proc. Natl. Acad. Sci. U.S.A.* **1978**, *75*, 5011−5014.

10.1021/ja0457563 CCC: $27.50

for cell division, and an excess of dGTP allosterically inhibits ribonucleotide diphosphate reductase, causing unbalanced deoxynucleotide pools and inducing apoptosis.[7−9] The discovery that hPNP activity is associated with T-cell function initiated an extensive development program for hPNP inhibitors that could moderate T-cell responses in the T-cell-associated disorders of T-cell leukemia, lymphoma, and rheumatoid arthritis, among others.[10]

It is well established that achieving the transition state (TS) is typically 10^{10} to 10^{15} times more probable in enzyme-catalyzed than in uncatalyzed reactions.[11] It has also been demonstrated that stable mimics of the TS which trap this energy of catalysis as stable binding energy have the potential to bind 10^{10} to 10^{15} times more tightly than reactant molecules. Experimental determination of different kinetic isotope effects (KIEs) provides an accurate geometrical depiction of the enzymatic TSs.[12−20] From this point, quantum chemistry calculations can be performed to obtain the theoretical KIEs, which are compared directly to the experimental ones, and this leads to a prediction of the TS structure, a blueprint for the design of potent inhibitors. In this fashion, an approximate transition-state structure for hPNP has been solved from experimental KIEs combined with computational chemistry studies.[21] Experimental KIE determination with inosine established that the TS is highly dissociative, with a notable separation between the ribosyl group and the departing purine ring. These studies led to the discovery of a family of TS analogues for hPNP, the immucillins, excellent mimics of the oxacarbenium TS (Figure 2). In principle, the immucillins can bind as the N-4′ neutral form like the natural substrates or as the N-4′ cationic form (N-4′ has a pK_a that permits formation of the cation at neutral pH). It has been postulated that ImmH binds to hPNP as the neutral species, and that in a subsequent step forms the cation.[22] Recent solid-state NMR studies have shown evidence that ImmH bound to hPNP is N-4′ protonated, to mimic the oxacarbenium TS.[23] Moreover, in the hPNP·ImmH·PO_4 (E·I) complex, N-7 captures a hydrogen bond to the enzyme that is a feature of the TS, but not of the Michaelis complex (the 9-deaza feature of the immucillins elevates the pK_a at N-7), as identified by X-ray crystallography and NMR

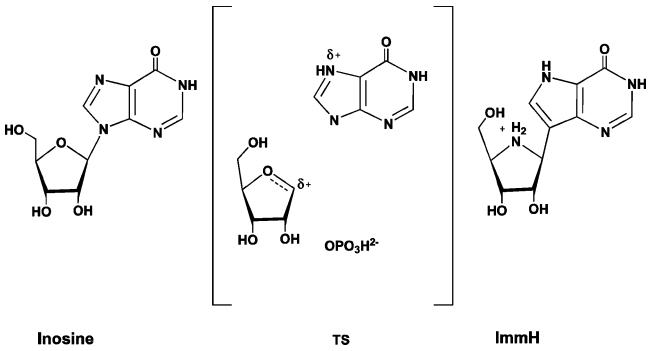

Figure 2. The transition state analogue ImmH resembles the positively charged oxacarbenium TS.

studies.[24] Additionally, the phosphoryl group in the E·I complex forms an ion pair with the TS analogue ImmH, and also appears to be highly nucleophilic on the basis of their ^{31}P chemical shifts.[23] Moreover, ^{31}P NMR and isotope-edited IR studies indicated that the P−O anharmonic vibrational mode of the nucleophile oxygen was decoupled from the other P−O bonds, having a lower anharmonic vibrational frequency.[25] This is another indication, together with the increased phosphate ionization,[23] that hPNP itself "activates" the phosphoryl nucleophile.

The cleavage of the C-1′−N-9 ribosidic bond occurs, as observed in many N-ribosyl transferase reactions, in a dissociative mechanism that forms a TS with a substantial oxacarbenium ion character. Little nucleophilic participation is observed at the saddle point; however, the phosphate provides an electrostatic stabilization of this oxacarbenium ion, encouraging TS formation.[21,26] After the TS is reached, there is substantial translocation of the ribosyl C-1′ toward the enzymatically anchored nucleophile. Moreover, as the N-ribosidic bond is cleaved and the pK_a values of the O-6 and N-7 atoms increase, electron density expelled by the oxygen-stack compression toward the purine ring improves electrostatic interactions with nearby residues and facilitates the abstraction of a proton from a close proton donor, makes the purine a better leaving group (hereafter "purine ring activation"), and accelerates catalysis. In summary, oxacarbenium stabilization, increased phosphate ionization, and purine ring activation contribute in concert to catalytic acceleration.

There is increasing evidence that, in certain reactions, motions within the protein itself speed the rate of a chemical step.[27−32] That is, certain motions of the protein couple strongly to a reaction coordinate, causing an increase in the reaction rate. Along these lines, we investigated how hPNP dynamics enhance the rate of the phosphorolysis reaction. We propose that protein-facilitated dynamic modes in hPNP and its substrates cause the O-5′, O-4′, and O_P oxygens to squeeze together and push

(6) Ullman, C.; Gudas, L. J.; Clift, S. M.; Jr., E. W. M. *Proc. Natl. Acad. Sci. U.S.A.* **1979**, *76*, 1074−1078.
(7) Schramm, V. L. *Biochim. Biophys. Acta* **2002**, *1587*, 107−117.
(8) Kicska, G. A.; Long, L.; Horig, H.; Fairchild, C.; Tyler, P. C.; Furneaux, R. H.; Schramm, V. L.; Haufman, H. L. *Proc. Natl. Acad. Sci. U.S.A.* **2001**, *98*, 4593−4598.
(9) Bantia, S.; Miller, P. J.; C. D. Parker, S. L. Annanth, L. L. H.; Kilpatrick, J. M.; Morris, P. E.; Hutchinson, T. L.; Montgomery, J. A.; Sandhu, J. S. *Int. Immunopharm.* **2001**, *1*, 1199−1210.
(10) Ealick, S. E.; Babu, Y.; Bugg, C.; Erion, M. E.; Guida, W. C.; Montgomery, J. A.; Secrist, J. A. I. *Proc. Natl. Acad. Sci. U.S.A.* **1991**, *88*, 11540−11544.
(11) Miller, B. G.; Wolfenden, R. *Annu. Rev. Biochem.* **2002**, *71*, 847−885.
(12) Rodgers, J.; Femec, D. A.; Schowen, R. L. *J. Am. Chem. Soc.* **1982**, *104*, 3263−3268.
(13) Cleland, W. W. *Methods Enzymol.* **1982**, *87*, 625−641.
(14) Northrop, D. B. *Biochemistry* **1975**, *14*, 2644−2651.
(15) Schramm, V. L. *Annu. Rev. Biochem.* **1998**, *67*, 693−720.
(16) Kline, P. C.; Schramm, V. L. *Biochemistry* **1992**, *31*, 5964−5973.
(17) Kline, P. C.; Schramm, V. L. *Biochemistry* **1993**, *32*, 13212−13219.
(18) Kline, P. C.; Schramm, V. L. *Biochemistry* **1995**, *34*, 1153−1162.
(19) Schramm, V. L. *Biochemistry* **1999**, *308*, 301−355.
(20) Fedorov, A.; Shi, W.; Kicska, G.; Fedorov, E.; Tyler, P. C.; Furneaux, R. H.; Hanson, J. C.; Gainsford, G. J.; Larese, J. Z.; Schramm, V. L.; Almo, S. C. *Biochemistry* **2001**, *40*, 853−860.
(21) Lewandowicz, A.; Schramm, V. L. *Biochemistry* **2004**, *43*, 1458−1468.
(22) Parkin, D. W.; Schramm, V. L. *Biochemistry* **1995**, *34*, 13961−13966.
(23) Sauve, A.; Cahill, S. M.; Zech, S. G.; Basso, L. A.; et al., A. L. *Biochemistry* **2003**, *42*, 5694−5705.
(24) Shi, W.; Lewandovicz, A.; Tyler, P. L.; Furneaux, R. H.; Almo, S. C.; Schramm, V. L. Crystal Structures of human purine nucleoside phosphorylase. Submitted for publication.
(25) Deng, H.; Lewandowicz, A.; Schramm, V. L.; Callender, R. *J. Am. Chem. Soc.* **2004**, *126*, 9516−9517.
(26) Schramm, V. L. *Acc. Chem. Res.* **2003**, *36*, 588−596.
(27) Antoniou, D.; Caratzoulas, S.; Kalyanaraman, C.; Mincer, J. S.; Schwartz, S. D. *Eur. J. Biochem.* **2002**, *269*, 3103−3112.
(28) Mincer, J. S.; Schwartz, S. D. *J. Phys. Chem. B* **2003**, *107*, 366−371.
(29) Mincer, J. S.; Schwartz, S. D. *J. Proteome Res.* **2003**, *2*, 437−439.
(30) Mincer, J. S.; Schwartz, S. D. *J. Chem. Phys.* **2004**, *120*, 7755−7760.
(31) Basner, J. E.; Schwartz, S. D. *J. Phys. Chem. B* **2004**, *108*, 444−451.
(32) Knapp, M. J.; Rickert, K.; Klinman, J. P. *J. Am. Chem. Soc.* **2002**, *124*, 3865−3874.

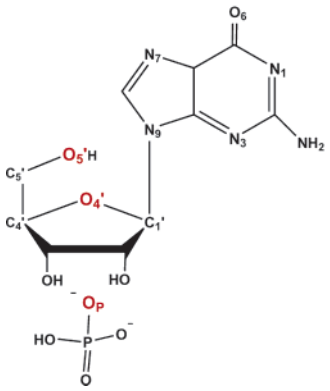

Figure 3. Atomic nomenclature of the purine nucleoside and phosphate nucleophile, with the O-5′, O-4′, and O_P atoms highlighted in red. The style follows the recommendations of IUPAC on biochemical nomenclature and terminology.

electrons toward the purine ring, stabilizing the oxacarbenium character of the TS. Furthermore, as the N-ribosidic bond is cleaved during the reaction, and the pK_a values of N-7 and O-6 increase, electron density expelled by these oxygens toward the purine ring facilitates the abstraction of a proton from a nearby residue, making the purine a better leaving group, and thus accelerating catalysis. Our hypothesis is based on the crystallographic evidence of several hPNP complexes with TS analogues, which showed an unusual geometric arrangement of the atoms O-5′, O-4′, and O_P, lying in a close three-oxygen stack (Figure 3), which was later corroborated by extensive experimental kinetic isotope effect (KIE) analysis.[20]

Hence, we investigated *nuclear protein-promoting vibrations* acting through geometrical changes and polar interactions. For the purpose of this study, we performed classical and mixed quantum/classical MD simulations of the Michaelis complex of hPNP and the substrates guanosine and phosphate, and monitored the O-5′−O-4′ and O-4′−O_P distances during the production run of the simulation, when the complex had fully equilibrated. Subsequently, we calculated the cross-correlation function of the O-5′−O-4′ and O-4′−O_P distances, as well as the distance autocorrelation function of O-5′−O-4′. Power spectra were obtained for these correlation functions. Moreover, to gain a better understanding of these molecular vibrations, an analogous analysis was done for the E·I complex, for the substrates guanosine and phosphate in aqueous solution, and for different hPNP mutants. The second part of this theoretical study examines if existing enzymatic vibrational modes in hPNP can actually be addressed as protein-promoting vibrations (PPVs), that is, if their coupling to the reaction coordinate has a direct impact on lowering the activation energy barrier. For this purpose, we performed quantum mechanical/molecular mechanical (QM/MM) calculations to obtain the potential energy surfaces (PESs) of several enzyme−substrate (E·S) structures extracted from the wild-type (WT) classical dynamics simulation, which showed great disparity in the O-5′, O-4′, and O_P oxygens' compression. In this manner, we obtained qualitative information on the amount of coupling of existing promoting vibrations with the reaction coordinate.

2. Methods

2.1. Enzyme Model. The starting point for the theoretical work was the 2.5 Å resolution structure of hPNP complexed with the TS analogue ImmH and phosphate.[24] Figure 4 shows the active site of hPNP and

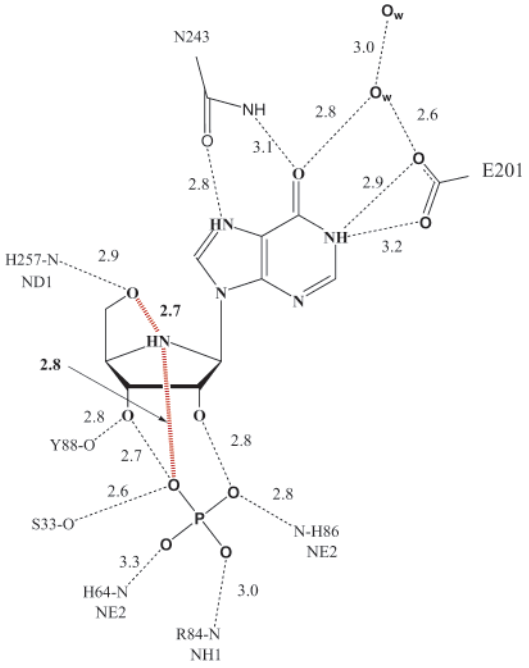

Figure 4. Structure of ImmH at the catalytic site of hPNP. Various site contacts of ImmH and the nucleophile with the active site residues are shown (Å).

ImmH, and we can observe that the O-5′, O-4′, and O_P atoms form a tight three-oxygen stack. The active site includes the residues S33, R84, H86, Y88, E89, F159, F200, E201, M219, N243, H257, and V260 and two catalytic waters (WAT502 and WAT520). All of these residues were strictly conserved among several sources of PNP, including human, bovine, mouse, and *Escherichia coli*. To make this modeling study practical in terms of CPU time, only one monomer of hPNP was used in our calculations, given that the three subunits are identical. We modeled guanosine from ImmH. Such an approach is feasible because ImmH closely resembles the oxacarbenium ion character of the TS. Some chemical modifications of ImmH were necessary to transform it into guanosine: The C-9 atom was substituted by N-9, and N-4′ by O-4′. The N-1-protonated tautomer of the base was chosen, as this is known to be present prior to catalysis in N-ribosyltransferases. The phosphate was modeled monoprotonated, its known ionization state in the complex.[23] All of its oxygens (except the nucleophilic) are hydrogen bonded strongly to S33, H64, R84, H86, A116, Y192, and a catalytic site water, which makes it perfectly anchored in the active site by the enzyme. Thus, only one phosphate oxygen, O_P, was less tightly bound and more nucleophilic than its counterparts, which is supported by IR studies.[25] The protonation state of all residues was assigned for the E·S complex with the Biopolymer module in the commercial package InsightII (Accelrys, San Diego, CA), according to the pK_a of their titratable groups, assuming a pH of 7. Finally, the model retained the 25 crystallographic water molecules. To relax any initial crystallographic strain, and allow the appropriate small geometric changes of the inhibitor ImmH as mutated into the natural substrate guanosine, minimization of the model was done using the CHARMM22[33] software package with a purely classical potential for all atoms.

To remove bad van der Waals contacts, 20000 cycles of steepest descent, followed by 3000 cycles with the adopted basis Newton−Raphson method with a step size of 0.2 Å, were performed, applying a weak restraining harmonic potential of 5 kcal mol^{-1} Å^2 to guanosine and phosphate to maintain them in their crystallographic positions, until the gradient of the energy converged. For the nonbonding interactions (electrostatic and van der Waals), we calculated the energy contributions

(33) Brooks, B. R.; Bruccoleri, R. E.; Olafson, B. D.; States, D. J.; Swaminathan, S.; Karplus, M. *J. Comput. Chem.* **1983**, *4*, 187−217.

for pairs of atoms within a cutoff of 12 Å, and we used a smoothing function to gradually reduce to zero this contribution between 12 and 14 Å. This final structure was the starting model for the WT MD simulation of the Michaelis complex of hPNP with the substrates guanosine and phosphate.

2.2. Classical Molecular Dynamics Simulations. The CHARMM22 all-atom parameter set was used for the standard amino acid residues for the MD simulations performed on the Michaelis complex of hPNP with guanosine and phosphate. MM point charges and parameters based on the CHARMM22 standard values were used for the substrates guanosine and phosphate. The TIP3P model represented the water molecules.[33] The SHAKE algorithm, with a tolerance of 10^{-8}, was applied to constrain all bonds involving hydrogen atoms.[34] The time step for the integration was 1 fs, sampling the trajectory every 5 fs. The temperature of the E·S complex was allowed to slowly increase over the first 10 ps from 0 to 300 K, and this temperature was maintained for the rest of the simulation. Initial velocities were assigned on the basis of a Gaussian distribution. After the heating phase, we allowed the system to equilibrate for 50 ps at 300 K, rescaling the velocities every 100 steps to the target temperature of 300 K, using a single scaling factor for all atoms. We used the same nonbonding interactions (electrostatic and van der Waals) as for the minimization. A constant dielectric was used. Finally, we continued the simulation for another 100 ps (production run), during which we collected the coordinates of the E·S complex every 5 fs.

In a similar manner, several classical simulations of mutated hPNPs were performed to assess the effect of the mutation of nearby residues on the three-oxygen-stack electronic interaction. In other words, we studied whether changes in protein structure have an influence on the modes of vibration observed in WT hPNP. The E201G, F200G, H257G, H257A, V260G, and L261G mutations were studied. For each simulation, the respective residue was manually mutated, the complex was minimized to accommodate the changes caused by the reduction of the mutated catalytic residue, and, subsequently, MD simulations were performed under conditions analogous to those of the previous WT hPNP simulation. Moreover, a classical simulation of the natural substrate guanosine and phosphate in a $40 \times 40 \times 40$ Å^3 box of TIP3P waters was also performed. With these simulations, we assessed the existence of any natural vibrations in the substrates guanosine and phosphate, and compared the frequencies in both enzymatic and nonenzymatic environments.

2.3. Hybrid Potential Dynamics Simulations. In addition to the classical simulations described in the last section, several hybrid potential simulations were performed. First, the E·S and E·I simulations were performed and directly compared to the purely classical E·S simulation. All the hybrid potential simulations were done with the CHARMM22 macromolecular simulation package, interfaced with the quantum chemistry program MOPAC 4.0 (Schrodinger, Inc., Portland, OR). In the QM/MM method, the effective Hamiltonian, H_{eff}, is the sum of three terms: H_{qm}, H_{mm}, and $H_{\text{qm/mm}}$. The H_{qm} term describes the quantum mechanical particles. The H_{mm} term is independent of the coordinates of the electrons and nuclei of the QM atoms. The $H_{\text{qm/mm}}$ combined Hamiltonian describes how QM and MM atoms interact. This is composed of an electrostatic term and a van der Waals term. Each MM atom (point charge) interacts with both the electrons and nuclei of the QM atoms; the van der Waals term is necessary since some MM atoms possess no charge and would consequently be invisible to the QM atoms, often providing the only difference in the interaction. For the simulations in our study, the enzymatic system was divided into two concentric zones. These consisted of the QM region, containing the atoms being treated quantum mechanically, and the MM region, in which the atoms were treated with a molecular mechanics potential. In the case of the simulation of the E·S complex, the QM region contained the substrates guanosine and phosphate and the conserved catalytic water WAT520. For the E·I complex, the QM region contained ImmG, phosphate, and WAT520. The AM1[35,36] semiempirical Hamiltonian was employed as the QM potential, and the all-atom force field of CHARMM22 was used to describe the atoms in the MM region. All the atoms in the quantum mechanical region were allowed to move freely during the simulations, and a small restraining force constant of 5 kcal mol^{-1} Å^2 was imposed on the nonquantum region, for reasons of convergence and speed. For the classical region, the SHAKE algorithm was used to constrain all bonds involving hydrogen atoms.[34] The time step for the integration was 1 fs. The temperature of the E·S complex was allowed to slowly increase over the first 20 ps from 100 to 300 K, and this temperature was maintained for the rest of the simulation. Initial velocities were assigned on the basis of a Gaussian distribution at 100 K. After a 20 ps heating phase, we allowed the system to equilibrate for another 100 ps at 300 K, during which the coordinates of the E·S complex were collected every 5 fs. We used analogous conditions to calculate the nonbonding interaction energy terms (electrostatic and van der Waals) as in the previous sections. A constant dielectric was used. For the QM region, an energy evaluation was done, and the first derivative was calculated to obtain the forces, required for the Verlet algorithm. The QM and MM regions interacted through the QM/MM energy term, which contains the interaction of all the point charges in the MM region with the electron density of the QM region and the nuclei for the same nonbond cutoffs set for the MM region in the classical MD simulations.

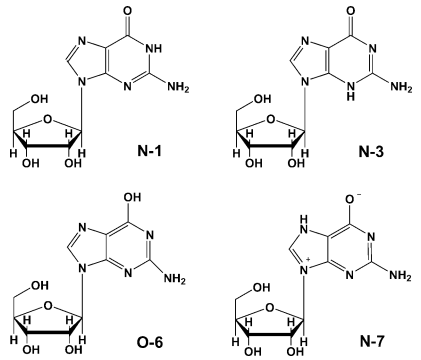

Figure 5. Four tautomers of guanosine used in the electronic structure calculations to investigate the relative energetics for the different protonation states of guanosine.

2.4. Preliminary Electronic Structure Calculations. Preliminary gas-phase electronic structure calculations were performed for a small version of the active site to acquire an initial mechanistic understanding of the importance of acid catalysis in the reaction. In this model, the nucleophile was modeled diprotonated because, in the absence of the eight strong hydrogen bonds present in the catalytic site, the phosphate is highly nucleophilic and liable to abstract even nonacidic protons from the nucleoside, leading to undesired side reactions. We performed calculations on the relative energy of the four tautomers of guanosine (Figure 5), and we computed the energy required to cleave the C-1′−N-9 ribosidic bond for the respective tautomers at the BHLYP/6-31G(d) level of theory. Similarly, we calculated the same energies required to break the N-ribosidic bond for two protonated tautomers at the same level of theory (Figure 6).

Furthermore, to choose the most accurate QM region for the computationally intensive QM/MM PES calculations, we performed gas-phase calculations of the phosphorolysis for different QM models. We found that the model which included the guanosine, the nucleophile, the conserved protonated water WAT520, and the residues N243 and E201 produced the most realistic energetics. This simplified model,

(34) Allen, M. P.; Tildesley, D. J. *Computer Simulation of Liquids*; Clarendon: Oxford, 1987.

(35) Dewar, M. J. S.; Thiel, W. *J. Am. Chem. Soc.* **1977**, *99*, 4899.
(36) Dewar, M. J. S.; Zoebisch, E. G.; Healy, E. A.; Stewart, J. J. P. *J. Am. Chem. Soc.* **1985**, *107*, 3902.

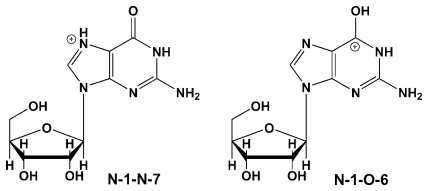

Figure 6. Two protonated tautomers of guanosine used in the electronic structure calculations to investigate the most likely protonation site of the purine ring during the phosphorolysis reaction.

which assumes a protonated water (hydronium ion), allows greater stabilization of the oxacarbenium TS via electrostatic interactions with the nearby catalytic residues and the electron-rich purine ring, and permits activation of the leaving group via strong hydrogen-bonding interactions/proton transfer to O-6 or N-7. The geometries of the corresponding stable structures and saddle points were fully optimized at the HF/3-21G(d) level of theory. Additionally, more accurate energetics were obtained by doing single-point energy calculations at the B3LYP/6-31G(d,p) level of theory based on the HF/3-21G(d) geometries. Vibrational frequencies were computed at the low level of theory to verify that the E·S and E·P were at minima on the PES. The TS was further characterized by a single imaginary frequency. The effect of zero-point energy (ZPE) for all bound vibrations was included in the energetics on the basis of the vibrational analysis at the same level of theory. All the calculations were performed with the commercial package Gaussian 98.[37]

2.5. Potential Energy Surfaces. The various minima in the PES of protein structures are well defined for E·S, E·I, or enzyme−product (E·P) complexes. A harder task involves the localization of the saddle points on the PES, which leads the reactant to products through the minimum energy pathway. Of increasing interest is the role that protein dynamic modes have on the modulation of the potential energy barrier that connects the reactant and product ground states. In the case of hPNP, we tested the hypothesis that these modes induce electronic changes which facilitate the chemical transformation taking place during the phosphorolysis reaction of guanosine.

The reaction mechanism of the enzyme was investigated using the QM(AM1)/MM layered method[38] to compute the PES using the interface of CHARMM22 and MOPAC 4.0. AM1, in common with other semiempirical molecular orbital methods, has acknowledged weaknesses in characterizing TSs.[39] Its accuracy in the present case has been established by comparison with preliminary high-level ab initio and DFT calculations on simple models of the reaction (see section 2.4). As an alternative to AM1, another MNDO-type method, such as PM3,[40] could have been used in the QM/MM calculations. AM1 and PM3 deal better with hydrogen-bonded systems than does MNDO[41] itself, but debate continues over the relative merits of these methods. For many applications, PM3 performs better than AM1. However, due to an apparent error in its parametrization, PM3 calculates charges for nitrogen atoms in N−H groups which are erroneously positive, leading to an incorrect description of the electrostatic potential of histidine. PM3 was also found to give poorer results for the enolate−enol reaction than AM1, compared to ab initio results.[39]

We chose a QM/MM model, denoted as QM/MM 1 (Figure 7), which included guanosine, the nucleophile, and the protonated conserved residue WAT520. Known mechanistic details of the reaction reveal that the purine ring accepts a proton from water or an unknown general acid, as the N-ribosidic bond is cleaved, prior to the formation of the TS. However, WAT520 is the only donor in direct contact with O-6, and no experimental data have yet characterized a catalytic acid residue;

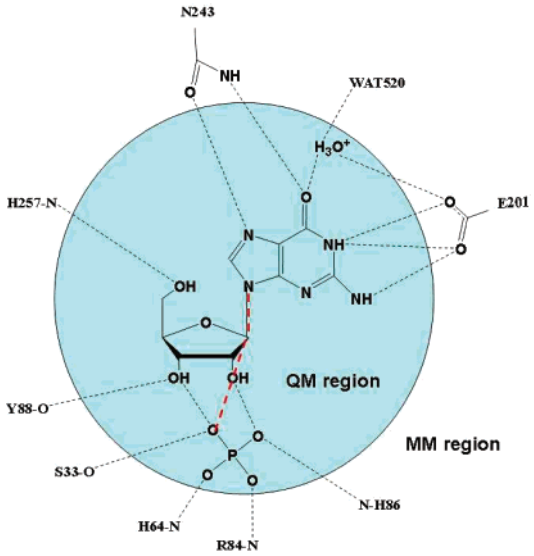

Figure 7. QM/MM 1 model used to obtain the PESs. The reaction coordinate used to produce these surfaces is shown with dashed lines in the figure.

thus, we assumed that a stepwise mechanism takes place, where a putative catalytic proton donor contributes a proton to the conserved residue WAT520 (assisted by the negatively charged E201, which draws the proton into the active site, and stabilizes the hydronium ion by positive electrostatic interactions), followed by proton transfer from the hydronium ion to the purine ring (assisted by N243 through favorable hydrogen bonds). Experimentally, replacement of N243 and E201 with alanine resulted in mutant proteins exhibiting catalytic efficiencies ca. 1000-fold lower than that of the wild type.[42] Moreover, these residues are actively involved in catalysis by stabilization of the TS. Yet, since they are not directly involved in the acid catalysis, they were not included in the QM region due to the limitations of these computationally expensive calculations. Nevertheless, their contribution to the stabilization of the TS structure is introduced by the QM/MM electrostatic term of the Hamiltonian. This study focused on the last step of the reaction, that is, the cleavage of the N-ribosidic bond and protonation of the purine ring to yield the protonated guanine and phosphorylated α-D-ribose. The QM/MM 1 model required no link atoms since no covalent bonds were broken between the QM and MM regions of the model. Test calculations on a QM/MM model containing guanosine, phosphate, and the unprotonated catalytic water WAT520 in the QM region produced rather high activation energies and failed to properly characterize the reaction studied. We reasoned that this model was not adequate because it lacked critical TS stabilization by favorable electrostatic interactions of the purine ring with adjacent residues; i.e., the unprotonated water residue did not succeed in forming strong hydrogen bonds with the O-6 and N-7 atoms. Furthermore, the QM/MM 1 model, as opposed to the test model, allowed protonation of the purine ring on O-6 or N-7 as the N-ribosidic bond is cleaved, making the purine ring a better leaving group (purine ring activation), and accelerating catalysis.

After investigating a variety of reaction coordinates, we found that suitable reaction coordinates to describe the phosphorolysis reaction were the interatomic C-1′−N-9 and C-1′−O_P distances (Figure 7). It is essential that a good reaction coordinate be used to represent the enzymatic reaction properly to obtain meaningful PESs. Calculating reaction paths for chemical or conformational changes in enzymes is a challenging problem because of the large size of the systems. This presents difficulties in characterizing saddle points and their associated pathways, because of the complex nature of protein PESs. We used an

(37) Frisch, M. J.; et al. *Gaussian 98*, Revision A.11.2; Gaussian, Inc.: Pittsburgh, 2001.
(38) Warshel, A.; Levitt, M. *J. Mol. Biol.* **1976**, *103*, 227−249.
(39) Mulholland, A. J.; Richards, W. G. A. *J. Phys. Chem. B* **1998**, *102*, 6635−6646.
(40) Stewart, J. J. P. *J. Comput. Chem.* **1989**, *10*, 209−220.
(41) Dewar, M. J. S.; Thiel, W. *J. Am. Chem. Soc.* **1977**, *99*, 4899−4907.
(42) Erion, M. D.; Stoecker, J. D.; Guida, W. C.; Walter, R. L.; Ealick, S. E. *Biochemistry* **1997**, *36*, 11735−11748.

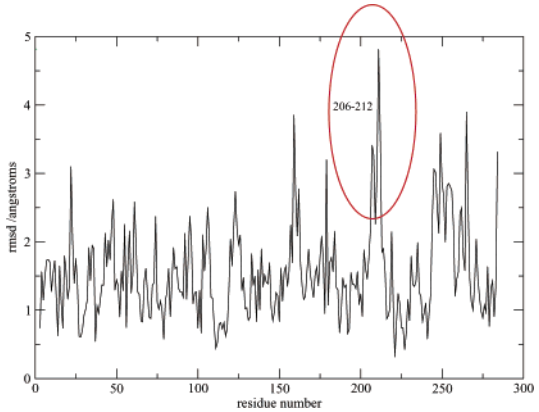

Figure 8. Average rmsd (Å) from the crystal structure of each residue over the WT classical MD simulation.

adiabatic mapping procedure, minimizing the total energy along this accurate reaction coordinate for each of the transformations. The adiabatic mapping approach is reasonable for proton/hydrogen/hydride transfers or covalent bond breakages, such as the one under consideration in this study, which is unlikely to be accompanied by major E·S conformational changes. To calculate the energetic profiles for a given reaction step, a harmonic restraint was applied to hold the selected reaction coordinate close to its value. We started breaking the C-1′−N-9 bond, from 1.4 to 4.0 Å, in steps of 0.025 Å. This was repeated for different C-1′−O_P distances, from 4.5 to 1.45 Å, in decrements of 0.025 Å, producing the PES of the phosphorolysis reaction. The force constant for restraining the C-1′−N-9 distance was 4500 kcal mol^{-1} $Å^{-2}$, a large value intended to keep the system close to the desired reaction pathway. These transformations were achieved by minimizing the whole system for a maximum of 2000 steps of the adopted basis Newton−Raphson method, or until the gradient of the energy converged below 0.001 kcal mol^{-1}. For the MM−MM nonbond interactions, we used conditions similar to those in the previous sections, and no cutoff was used for the QM−MM interactions. A mass-weighted restraint of 10 kcal mol^{-1} $Å^{-2}$ was imposed on the nonquantum region during the reaction path calculations. Each TS was finally located on the PES, and vibrational analysis was performed to verify this as a saddle point. We tested our hypothesis by analyzing 11 E·S configurations obtained from the WT classical dynamics which presented disparate O-5′−O-4′−O_P distances, and compared the barrier heights for each structure.

3. Results

3.1. Molecular Dynamics Simulations. During the production run of the classical dynamics simulation of the E·S of hPNP and guanosine and phosphate, we observed that certain residues were relatively mobile. Figure 8 shows the average root-mean-square deviation (rmsd) from their crystal structure of each residue over the 100 ps production run. We take special notice of the high mobilities of residues 206−212 and the two catalytic water molecules WAT502 and WAT520 (not shown), another cue that these residues may be involved in shuttling the proton between the putative catalytic acid and the purine ring.

Figure 9 shows the O-5′−O-4′ and O-4′−O_P distances throughout the classical MD simulation. We can see that these distances are quite stable, deviating up to 0.3 Å from the average value. For example, the O-5′−O-4′ distance achieves values in the range of 2.5−3.2 Å. This is implicit evidence that the O-5′−C-5′−C-4′−O-4′ dihedral angle is not rotating freely as it does in aqueous solution, but is "restricted" by the enzymatic environment. Figure 10 depicts the dihedral angle in the enzymatic environment and in aqueous solution over a period

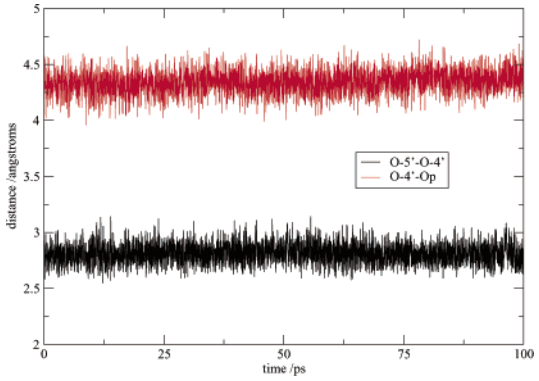

Figure 9. O-5′−O-4′ and O-4′−O_P distances (Å) during the WT classical MD simulation.

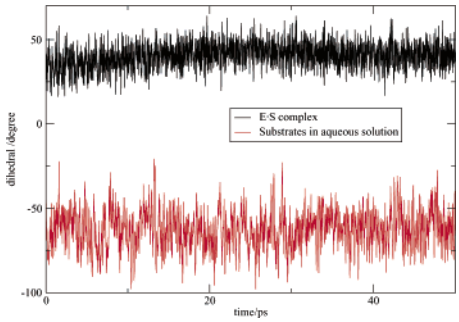

Figure 10. O-5′−C-5′−C-4′−O-4′ dihedral angle (deg) of the ribose ring during the WT classical MD simulation in aqueous solution and in the E·S complex.

of 50 ps. We can see that the mean value in each case is different; moreover, there is a higher deviation of this dihedral angle from its mean value in solution.

The results of the classical dynamics simulations for the mutated hPNPs presented in Table 1 show the average O-5′−O-4′ and O-4′−O_P distances and standard deviations for the WT and for several mutants of hPNP complexed with guanosine and phosphate. The changes in compression of the oxygen stack for each mutated form of hPNP varied for each mutation. We found that, for H257G and H257A, the average O-5′−O-4′ distance was considerably higher than that of the WT (note that, throughout the simulation, the O-5′−O-4′ distance only fluctuates between 2.6 and 3.2 Å (Figure 9); consequently, a difference of 0.2 Å in the average O-5′−O-4′ distance is a substantial difference).

Subsequently, we extracted the coordinates of the E·S complex every 5 fs during the production run of the simulation. We computed the O-5′−O-4′ and O-4′−O_P interatomic distances every 5 fs of the simulation for a total of 100 ps. The O-5′−O-4′ distance autocorrelation function and the O-5′−O-4′ and O-4′−O_P distance−distance cross-correlation function were calculated. The Fourier transforms (FTs) of these correlation functions were very similar, showing that O-5′−O-4′ and O-4′−O_P vibrate at the same frequencies: 125 and 465 cm^{-1} in the enzyme environment (Figure 11), which translate into 500−1500 fs motions.

To obtain insight into how much these vibrations are effected by hPNP or if they are inherent in the substrates, we performed an analogous classical dynamics simulation of the substrates in the absence of hPNP in aqueous solution. The FT of the O-5′−O-4′ distance autocorrelation function of the classical MD of

Table 1. Average O-5′−O-4′ and O-4′−O_P Distances (Å) for the WT and the Mutated hPNPs

distance	WT	F200G	E201G	V260G	L261G	H257G	H257A
O-5′−O-4′	2.81 ± 0.08	3.04 ± 0.08	2.88 ± 0.11	2.78 ± 0.08	2.88 ± 0.09	3.04 ± 0.08	3.02 ± 0.11
O-4′−O_P	4.34 ± 0.10	4.32 ± 0.12	6.58 ± 0.11	3.90 ± 0.11	4.01 ± 0.12	4.69 ± 0.10	4.35 ± 0.14

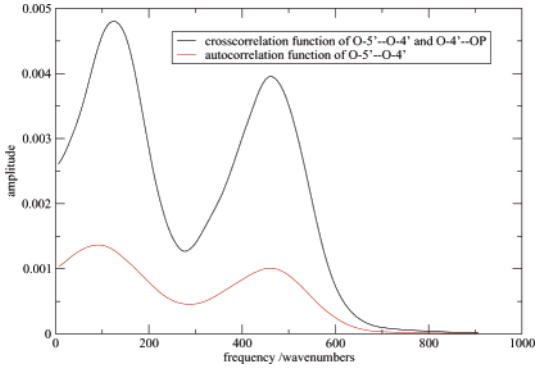

Figure 11. Comparison of the power spectra of the O-5′−O-4′ distance autocorrelation function and the O-5′−O-4′ and O-4′−O_P distance−distance cross-correlation function.

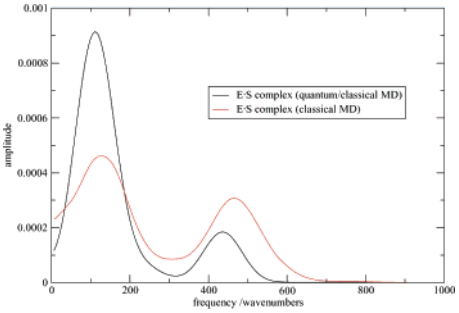

Figure 12. The power spectra of the O-5′−O-4′ distance autocorrelation function for the E·S complex based on the classical and quantum/classical MD simulation show an agreement of both purely classical and hybrid simulations as observed from the resonance of the peaks.

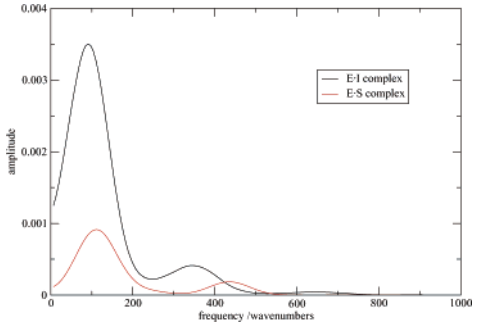

Figure 13. The power spectra of the O-5′−O-4′ distance autocorrelation function for the E·S and E·I complexes based on the quantum/classical MD simulation show that hPNP also effects the PPV with ImmG though the reaction does not take place by virtue of the chemical stability of the TS analogue.

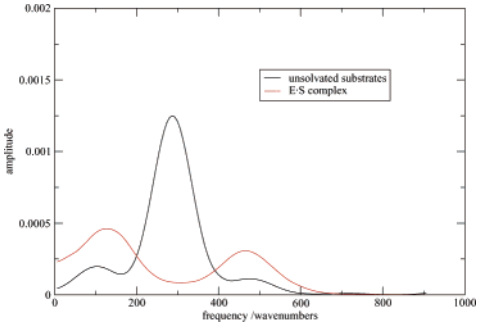

Figure 14. Power spectra of the O-5′−O-4′ distance autocorrelation function for hPNP and unsolvated substrates. We can observe that the natural vibration of the oxygen centers, i.e., 285 cm^{-1}, is altered in the presence of the enzyme.

solvated substrates showed a peak at 330 cm^{-1}, and that of the unsolvated substrates showed a peak at 285 cm^{-1}. Figure 14 shows the power spectra of the O-5′−O-4′ distance autocorrelation function for hPNP and unsolvated substrates. Furthermore, the power spectrum of the quantum QM(AM1)/MM simulation of E·S reproduced the peaks of the purely classical dynamics simulation. Figure 12 shows the power spectra of the E·S for the classical and mixed quantum/classical MD simulations, and Figure 13 shows those of the E·S and E·I based on the hybrid simulation production run.

We can observe that, even in the E·I complex (with the ImmG inhibitor), O-5′−N-4′ naturally tends to vibrate at frequencies similar to those of O-5′−O-4′ in the E·S complex. However, the PPV in the E·I complex does not take place by virtue of the chemical stability of the C-1′−C-9 bond. In summary, in the catalytic site, the O-5′, O-4′, and O_P oxygens vibrate at two specific frequencies, and this observed behavior is altered in the absence of the enzyme environment, revealing that hPNP is directly affecting the way in which these oxygens naturally vibrate.

In a similar manner, several classical simulations of mutated hPNPs were performed to assess the effect of the mutation of nearby residues on the three-oxygen-stack electronic interaction. In other words, we studied whether changes in protein structure have an influence on the modes of vibration observed in WT hPNP. Thus, for the F200G, E201G, H257G, H257A, V260G, and L261G mutated simulations, an analogous analysis was performed. The power spectrum of the O-5′−O-4′ distance autocorrelation corresponding to the F200G, E201G, V260G, and L261G mutated hPNPs was very similar to that of the WT. In contradistinction, the H257G was very similar to that of the unsolvated substrates, giving further evidence that H257 is responsible for modifying the power spectrum in the E·S complex. Surprisingly, the power spectrum of the H257A mutation was not analogous to that of H257G but rather appears to be a mixture of that of the WT and that of H257G, as shown by the power spectra in Figure 15. This indicates that the direction by H257 of the lone pair of O-5′ toward O-4′ of guanosine is of a mechanical rather than electronic nature, but as we will show, while the "push" by H257 is mechanical, its effect on the catalytic mechanism is electronic. This is another case of nuclear protein-promoting vibrations recently characterized in enzymes such as liver alcohol dehydrogenase (LADH),[27,31,43] in which the PPV is effected through polar interactions from the geometrical alterations of the three atom centers.

(43) Antoniou, D.; Schwartz, S. D. *J. Phys. Chem. B* **2001**, *105*, 5553−5558.

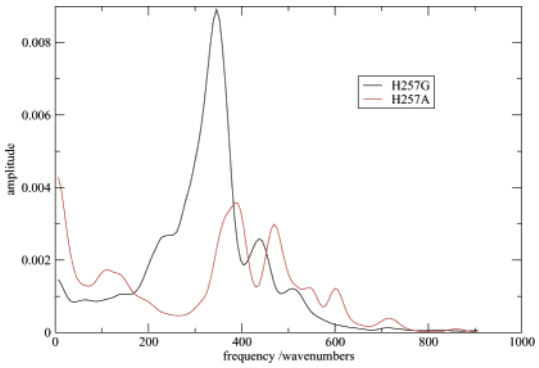

Figure 15. The power spectra of the H257G and H257A mutants of the E·S complex show a distinct peak at 333 cm^{-1} for the H257G mutant, mimicking that of the substrates in the absence of hPNP. However, the H257A mutant shows nascent peaks at 125 and 465 cm^{-1} similar to those of the WT complex, suggesting that the H257G mutation is more effective than H257A in modifying the natural vibration of the oxygen centers.

To study the degree of coupling of the PPV to the electronic fluctuation (Mincer, Núñez, et al., manuscript in preparation), we monitored the charge fluctuations in the ribose and purine groups separately throughout the simulation. We calculated these partial charges of the nucleoside for 1000 snapshots during the MD trajectory. Subsequently, time series were generated for each atom, with its partial charge a function of simulation time, and power spectra were generated for the ribose and purine ring partial charge time series. The results demonstrated that charge fluctuations in the ribose and purine ring groups are resonant with the PPV (peaks are seen at ca. 160 and 450 cm^{-1}), and support our findings that the PPV effects an electronic rearrangement in the nucleoside by stacking the three-oxygen stack close together.

3.2. Electronic Structure Calculations. We performed gas-phase electronic structure calculations to assess the importance of acid catalysis in the reaction. The results of the calculations at the BHLYP/6-31G(d) level of theory of the unprotonated tautomers of guanosine (Figure 5) concluded that the relative energies of the N-1, N-7, and O-6 tautomers compared to the N-3 tautomer are ca. 5.7, 21.1, and 18.5 kcal mol^{-1}, respectively. Additionally, the activation energies for the phosphorolysis reaction were found to be approximately 31.2, 28.6, 45.4, and 36.2 kcal mol^{-1} for the N-1, N-7, N-3, and O-6 tautomers. In the case of the two protonated tautomers (Figure 6), the N-1−N-7 tautomer was more stable by ca. 12 kcal mol^{-1} than N-1−O-6, and breaking the N-ribosidic bond required ca. 25.0 and 14.3 kcal mol^{-1} for the N-1−O-6 and the N-1−N-7 tautomers, with TS imaginary frequencies of 155i and 198i cm^{-1}, respectively, at the same level of theory (ZPE corrections were not included). This reveals important information about the mechanism. First, it agrees with known nucleoside chemistry, where the energetic requirement to break the N-ribosidic bond is less costly when the purine ring is protonated. Second, when the reaction proceeds without protonation of the purine ring, phosphorolysis is more favorable for the N-1 and N-7 tautomers of guanosine, which is in agreement with experimental data and validates the model of guanosine used in this study. Finally, the calculations on the N-1−N-7 and the N-1−O-6 protonated tautomers of guanosine suggest that the reaction is slightly faster for the N-1−N-7 than N-1−O-6 tautomer, supporting protonation of the purine ring by an external source at N-7. Special care must be taken with gas-phase calculations. In the enzyme, the pK_a values of the different atoms of the purine ring will be slightly affected, and so will the energetics/mechanism of the reaction. Therefore, these calculations are useful for obtaining qualitative understanding of the reaction, though they are not conclusive, and a QM/MM study must follow.

Table 2. Activation Energies (kcal mol^{-1}) and Distances (Å) of the E·S and E·TS Complexes (in Parentheses) for 11 Structures Taken from the Production Run of the WT Classical MD Simulation

structure	E_a	C-1′–N-9	C-1′–O_P	O-5′–O-4′	O-4′–O_P
1	46.3	1.45 (2.27)	3.08 (2.17)	3.11 (2.97)	3.62 (2.71)
2	48.5	1.45 (2.25)	3.22 (2.18)	2.86 (3.02)	3.62 (2.61)
3	46.1	1.44 (2.22)	3.95 (2.30)	2.78 (3.11)	4.25 (2.66)
4	53.1	1.44 (2.30)	4.29 (2.40)	2.93 (3.06)	4.30 (2.80)
5	49.1	1.45 (2.32)	3.17 (2.15)	2.88 (2.94)	3.49 (2.58)
6	56.6	1.44 (2.35)	4.04 (2.28)	3.25 (3.34)	4.30 (2.84)
7	47.7	1.45 (2.35)	3.07 (2.15)	3.64 (3.64)	3.35 (2.65)
8	52.0	1.45 (2.30)	3.86 (2.25)	3.12 (3.16)	4.24 (2.75)
9	50.6	1.44 (2.30)	3.74 (2.20)	3.08 (3.08)	3.81 (2.64)
10	48.4	1.45 (2.30)	3.33 (2.20)	3.11 (3.14)	3.73 (2.71)
11	51.9	1.44 (2.35)	3.49 (2.17)	3.19 (3.19)	3.85 (2.70)

Additionally, we investigated a suitable model for the characterization of the phosphorolysis reaction and production of PESs and considered the model which included the substrates, protonated WAT520, N243, and E201. On the basis of the former results, which show the importance of acid catalysis for the reaction studied, we decided to include the protonated conserved water residue WAT520 in the QM region to allow a better stabilization of the electron-rich leaving group. At the B3LYP/6-31(d,p)//HF/3-21G(d) level of theory, the preferred reaction pathway is a concerted phosphorolysis reaction, with activation and reaction energies of 36.6 and 13.1 kcal mol^{-1}, respectively, and an imaginary TS frequency of 430i cm^{-1}. These preliminary results suggest that the model shown in Figure 7 is suitable to study the phosphorolysis reaction under consideration. Thus, we regard it as a solid model for the subsequent investigation of the magnitude of the coupling of the PPV and the reaction coordinate, using the hybrid QM/MM method.

3.3. Potential Energy Surfaces. To assess the extent to which the PPV is positively coupled to the reaction coordinate, we utilized the hybrid QM/MM method to obtain the potential energy surfaces for the phosphorolysis reaction for various E·S complexes which presented a range of O-5′−O-4′ and O-4′−O_P interatomic distances. The results of the QM(AM1)/MM reaction path calculations are shown in Table 2. The table shows the activation energies (kcal mol^{-1}) and interatomic distances (Å) of the E·S complex, and in parentheses, the corresponding values for the E·TS complex. Vibrational analysis was performed to locate the imaginary frequencies of the E·TS complexes, which were ca. 250i cm^{-1}.

We present several structures, labeled 1−11, which correspond to increasingly longer times, taken from the production run of the WT classical MD simulation. Specifically, they range from 9.2 to 96.42 ps in our 100 ps ensemble of structures. The collection of E·S we chose embraces a wide range of geometries, with O-5′−O-4′ ranging from 2.78 to 3.64 Å and O-4′−O_P ranging from 3.35 to 4.30 Å. Thus, these 11 structures were sufficient to represent the different E·S geometries that can be found in the PES. We can see that the activation energies also varied from 46.3 to 59.9 kcal mol^{-1}. One might argue that these activation energies are rather large. A pausible explanation may

be that protonation of the purine ring never takes place during the reaction, as opposed to experimental predictions that protonation of the leaving group happens before formation of the TS structure. Unfortunately, the semiempirical Hamiltonian (AM1) used to model the bond-breaking/bond-making event did not succeed in characterizing N-7 or O-6 protonation; therefore, the augmented energetics are observed. Nonetheless, AM1 is appropriate to calculate relative energetics for this reaction, regardless of not characterizing the purine ring protonation or overestimating the absolute activation energies, since it is consistent with high-level ab initio and DFT energies and geometries. Therefore, we obtained an E·TS ensemble which is less dissociative than the "true" E·TS ensemble, that is, a E·TS ensemble where a proton has fully transferred to N-7 or O-6. We emphasize that this study is not intended to predict exact energies, nor to understand the catalytic acid/source of the proton, but rather to investigate one of the factors of efficient catalysis, that is, the effect of the three-oxygen compression on the barrier height. Although this preliminary study is adequate to investigate the relative importance of PPVs in hPNP by comparison of relative potential energy barriers at the QM(AM1)/MM level of theory, a subsequent study at a higher level of theory (possibly using DFT or AM1-SRP to describe the atoms in the QM region) will be necessary to show more reliable energetics for the reaction.

From the 11 E·S complexes analyzed, we observed that, after the TS is achieved, which normally happens at C-1′−N-9 and C-1′−O_P distances of 2.3 and 2.2 Å, respectively, continued atomic motion causes progression of the reaction coordinate motion toward products by the excursion of the ribose ring toward the environmentally fixed nucleophile. A surprising feature of this mechanism is that the enzyme provides no near-neighbor contacts to C-1′, the site of oxacarbenium ion formation. In the complex of hPNP−ImmH−phosphate, the nearest neighbor to N-4′ is 2.7 Å away, and 2.9 Å from the hydroxyl O-5′ oxygen is H257. On the opposite side of this group is the nucleophile oxygen O_P at 2.8 Å. We have previously shown that the phosphate nucleophile has substantially favorable electrostatic interactions in the E·S complex, via the O-4′−O_P interaction (Figure 3). Furthermore, it is also crucial for the formation of the E·TS complex, providing favorable stabilizing electrostatic interactions with the oxacarbenium TS.

In Figure 16 we plot the activation energies for the phosphorolysis reaction vs the sum of the O-5′−O-4′ and O-4′−O_P distances. From Figure 16 and Table 2, we see a correlation between short O-5′−O-4′ and O-4′−O_P distances and low activation energy, i.e., the higher the sum of these two distances in the E·S complex (and to a lesser extent in the E·TS complex, not shown), the higher the activation energy of the phosphorolysis reaction.

To quantify this correlation between lower activation energy and compression of the oxygen distances, we fitted the data of Figure 16 to three different functions: to a straight line, to a parabola with linear and quadratic terms, and to a parabola with a quadratic term only. From the value of χ^2, we found that the two parabolic fittings were about equally good, but the fitting to a straight line had a higher χ^2.

The parabolic dependence of the activation energy on distance may have a simple interpretation: as the distance between the oxygens increases the energy rises as carbocation stabilization

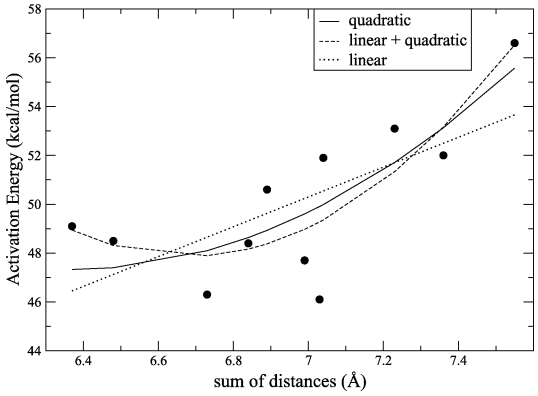

Figure 16. Activation energies (kcal mol^{-1}) versus the sum of O-5′−O-4′ and O-4′−O_P distances (Å) for the E·S complex. We show three fittings to the data: linear fitting (dotted line), parabolic fitting with only a quadratic term (solid line), and parabolic fitting with both linear and quadratic terms (dashed line). The calculated values of χ^2 show that the two parabolic fittings are equally good and better than the linear fitting. The second parabolic fitting captures the feature that there is a small increase of activation energy at very short distances, which could be attributed to strong electronic repulsion at short distances.

is lost, but at shorter distances, as we approach distances equal to twice the van der Waals radius, electron−electron repulsion will compete with the stabilization, and there is a point where there is no further reduction of the activation energy. From the values of the curvature of the parabolic fittings we can obtain a spring constant, and by using a mass equal to the reduced mass of O−O, we can obtain an effective harmonic frequency associated with the parabolic fittings shown in Figure 16. This effective frequency was equal to 130 cm^{-1} for the parabolic fitting with only a quadratic term, and 180 cm^{-1} for the parabolic fitting with both linear and quadratic terms. These values of the harmonic frequency are in remarkable agreement with the position of the peaks in the spectra of the autocorrelation functions of O−O distances shown in Figures 11 and 12. Of course, this interpretation of the activation energy as depending harmonically on the oxygen distances is not rigorous, but it is reassuring that it gives an effective frequency that has the same order of magnitude as the vibration we expected to promote the rate.

From these results, we conclude that the PPV can be considered as one of the factors which makes the reaction possible, and that this effect can lead to up to a 20% decrease in barrier height.

To obtain catalytically relevant insight into the active site residues, we measured interatomic distances between N243, E201, H257, and WAT520 and the purine ring. E201 is a crucial residue, and it is likely to have a role in stabilizing the positive charge of the incoming proton into the active site. Interactions from E201 are important for leaving group activation, since E201A causes a 10000-fold decrease in k_{cat}.[42] The hydrogen bond from the carboxyl of E201 to N-1 remains highly favorable at 2.8−2.9 Å throughout the reaction coordinate, similar to the 2.6−2.7 Å hydrogen bond between the same carboxyl oxygen and the highly conserved water molecule WAT520, which we hypothesize acts as the specific acid catalyst by a strong hydrogen bond to O-6 at the TS. Interactions from N243 are unequivocally important for transition-state stabilization and leaving group activation. We showed in a previous section that N243 is rather mobile compared to the other catalytic residues. During the MD simulation, N243 is able to form hydrogen bonds

with N-7, O-6, and WAT520, directly participating in TS stabilization and leaving group activation. Furthermore, we pose the question of whether N243 is directly involved in shuttling the transferring proton. Along these lines, it has been recently found experimentally that the vibrational C-6−O-6 stretching mode is 1685 cm^{-1} in aqueous solution, as opposed to the 1655 cm^{-1} stretch of the carbonyl group of ImmH bound to hPNP (Deng, H., unpublished results). This could be interpreted as a strong hydrogen bond to WAT520 or even a partially transferred proton to O-6, which increases leaving group activation, as observed in crystallographic studies.[24] Though preliminary electronic structure calculations of a simplified model in the gas phase showed that proton transfer to O-6 is less favorable than to N-7 by ca. 10 kcal mol^{-1}, in the enzymatic environment, where the pK_a values of the atoms may be shifted by the environment, proton transfer to O-6 is viable since the protonated O-6 can be readily stabilized by N243, the catalytic water WAT520, and E201. This mechanism is supported by experimental vibrational analysis which showed that the C−O carbonyl vibrational frequency of ImmH is lower in the presence of hPNP as compared to that in aqueous solution (Deng, H., unpublished results). This or another proton may also transfer to N-7 via N243, in that manner corroborating the multiple catalytic roles of N243.[42] Future studies shall focus on investigating how the proton transfers from the outer part of the active site to the purine ring vicinity. Experimental site-directed H257G mutagenesis causes a ca. 20-fold decrease in k_{cat}/K_M (Lewandowicz, A., unpublished results) of the phosphorolysis reaction of inosine (we expect similar kinetic data for the phosphorolysis of guanosine), and supports our findings that H257 is an important residue in the phosphorylation reaction catalyzed by hPNP. Specifically, H257 is not directly involved in acid catalysis (transfer of the proton into the active site/protonation of the leaving group as N243 or E201), though it does have an important role in the binding of the nucleoside and fixing the 5′-hydroxyl in the geometry of the ribosyl group. That is, we have seen from the crystal structures available of the different complexes of the hPNP with the potent inhibitors in the immucillin family, and from our MD simulations, the O-5′−C-5′−C-4′−O-4′ dihedral angle does not deviate much from that found in the crystal structure, always at a small distance from O-4′, and that this trait is reversed when the substrate guanosine is free in solution, where the O-5′−C-5′−C-4′−O-4′ dihedral angle adopts a wider range of values and is not restricted as in the enzyme.

4. Concluding Discussions

We have investigated nuclear PPVs in hPNP. Crystallographic observations of hPNP with several TS analogues in the immucillin family showed an unusual geometric arrangement of the atoms O-5′, O-4′, and O_P, the nucleophilic phosphate oxygen, lying in a close three-oxygen stack.[24] These observations were corroborated by extensive experimental KIE analysis.[20] Our hypothesis that dynamic oxygen compression is one component of the catalytic power of this N-ribosyltransferase to facilitate formation of the oxacarbenium TS is supported by MD and QM/MM−MD calculations. Electron flow to reach this TS involves loss of electrons from the O-4′ oxygen to form a partial double bond to C-1′, rehybridization of C-1′ toward sp^2 geometry, loss of bonding electrons into the purine leaving group, and assistance for the purine ring to accept bonding electrons by protonation and/or strong hydrogen bonds to O-6 and N-7. Moreover, we have shown that the strictly conserved H257 residue in the vicinity of O-5′ is responsible for creating this squeezing motion, concluding that this PPV is coupled to efficient catalysis.

Acknowledgment. We thank the National Science Foundation Chemistry Division (Grant CHE-0139752 (S.D.S., S.N.)), the Office of Naval Research (Grant N00014-00-1-0097 (S.D.S., S.N.)), and the National Institutes of Health (Grants GM41916 and GM068036) for support. We also thank the Bioinformatics Group at the Albert Einstein College of Medicine and Prof. Jiali Gao at the University of Minnesota MSI for computing time.

JA0457563